A&A, 687, A167 (2024)
https://doi.org/10.1051/0004-6361/202449379

Astronomy & Astrophysics

An approach to the effects of stellar rotation on the theoretical apsidal motion constants

Calculations from 0.40 $M_\odot$ to 25.0 $M_\odot$

A. Claret[1,2]

[1] Instituto de Astrofísica de Andalucía, CSIC, Apartado 3004, 18080 Granada, Spain
e-mail: claret@iaa.es
[2] Dept. Física Teórica y del Cosmos, Universidad de Granada, Campus de Fuentenueva s/n, 10871 Granada, Spain

Received 29 January 2024 / Accepted 19 April 2024

ABSTRACT

Aims. The most reliable sources for determining absolute stellar parameters are the double-lined eclipsing binary systems. Some of these systems also show apsidal motion, characterized by the variable log k_2. This point grants us the possibility of investigating the stellar interior, specifically the degree of stellar mass concentration. The first studies carried out about four decades ago on this topic showed appreciable discrepancies not only with respect to the comparison between the observed absolute dimensions and their theoretical counterparts, but mainly concerning the degree of mass concentration through the analysis of their apsidal motions. Fortunately, this scenario has been gradually improving with the advances in the quality of observational techniques and advances in the input physics of the evolutionary stellar models (e.g. opacities, thermonuclear reactions, equations of state, numerical techniques). These new developments in the input physics has improved the comparison between observations and the values predicted by theory, including the apsidal motion rates. This progress has lead us to investigate second-order effects such as rotation and dynamic tides. In this paper we deal with the effects of rotation on the degree of mass concentration.
Methods. The stellar models were calculated using the MESA package. The mass range studied here was 0.40–25.0 $M_\odot$ for a generic chemical composition characterized by $X = 0.70$ and $Z = 0.02$. The present models were computed without taking into account core overshooting in order to highlight the effects of rotation. Each model was followed from the pre-main sequence until the central hydrogen content is of the order of or less than 0.03, covering the range of masses and evolutionary status of the double-lined eclipsing binaries showing apsidal motion. Regarding the calculation of the internal structure coefficients, we integrated the Radau equation using the fifth-order Runge-Kutta method and a tolerance level of 10^{-7}. As an auxiliary tool, homology transformations have been used to explain, qualitatively, how the equation of state, thermonuclear reactions, and convection impact the degree of mass concentration of the models.
Results. In our past studies on the effects of rotation on log k_2 an average correction was used for all models together. For this a small range of masses (2.0, 7.0, 15.0 $M_\odot$) has been used. In the present paper the corrections due to the effects of rotation in log k_2 are presented for each mass individually and for three evolutionary phases. This point is particularly important, given that these corrections show a clear dependence on the mass and on the evolutionary status. Such corrections can be easily introduced into the theoretical calculation of apsidal motion rates through a linear equation. A typical correction due to the rotation effects is of the order of −0.03 in log k_2.

Key words. binaries: eclipsing – stars: evolution – stars: interiors – planetary systems – stars: rotation

1. Introduction

Double-lined eclipsing binary systems (DLEBSs) are the most reliable and accurate sources for obtaining absolute dimensions of stars (a few per cent error in masses and radii and, in a few cases, even of the order of 1%). On the other hand, the study of apsidal motion rates for this kind of binary system gives us the possibility to investigate in detail the stellar interior, particularly how the mass is distributed as a function of radius through the apsidal motion constant log k_2. The need for high precision in absolute dimensions for this kind of study comes from the fact that theoretical apsidal motion rates depend strongly on the stellar radii (fifth power), the masses of both components, their angular velocities, the observed eccentricity, and log k_2, and their respective observational and theoretical errors. As examples of the precision of observational data to carry out apsidal motion analysis, see Tables 1 and 3 in Claret et al. (2021).

Concerning the confrontation of theoretical and observational values of log k_2, large discrepancies were detected about 40 years ago. That disagreement was, in part, due to the quality of observational data, but mainly came from the theoretical models of stellar evolution that were often unable to fit even the actual effective temperatures and log g for a given DLEBS, the first stage of the apsidal motion analysis process. The results of these analyses showed a clear disagreement between the observational data and the theoretical calculations in the sense that the models were less mass concentrated than their observed counterparts (for a brief historical review on this point, see e.g. Claret & Giménez 1993).

In the last two decades studies on the stellar interiors using apsidal motion in DLEBSs have greatly improved the agreement between the theoretical values and the observational data. To the best of our knowledge, the last systematic study on the comparison between theoretical and observational rates of apsidal motion was

carried out by Claret et al. (2021). In that research 27 DLEBSs were used, whose minimum times were extracted from the light curves using the Transiting Exoplanet Survey Satellite (TESS). A good agreement was found between theory and observational data concerning absolute stellar dimensions and for the apsidal motion rates. The physical phenomena that, under the theoretical point of view, was key to reaching such a good inter-agreement was the introduction of core overshooting in the evolutionary stellar models. The models computed adopting this option are more concentrated in mass (smaller log k_2). However, Claret & Torres (2019) and the papers quoted therein show that the amount of core overshooting necessary to adjust the absolute dimensions of selected DLEBSs are limited to masses of the order of 4.0 $M_\odot$. This limitation is due to there not being enough accurate observational data for more massive systems sufficiently evolved for the effects of core overshooting to be appreciable, such as late stages of the main-sequence or giant phase.

Considering the current status of apsidal motion studies, we think it would be interesting to focus on second-order effects here, such as the influence of rotation on the degree of mass concentration. Historically, the first evolutionary models computed integrating the Radau equation taking rotation into account were those due to Stothers (1974). That author adopted only homogeneous configurations and uniform rotation. The correction in log k_2 by rotation found by Stothers was $-0.7\ \lambda$. In such an expression $\lambda = 2V^2/(3gR)$, where V is the equatorial rotational velocity, g the surface gravity, and R the stellar radius. Years later Claret (1999), using the formalism by Endal & Sofia (1976) incorporated into the GRANADA code, computed rotating models for 2.0, 7.0, and 15.0 $M_\odot$ to study the effects of rotation on log k_2. That author performed calculations for three evolutionary phases: $X_c = 0.70$, 0.35, and for the red hook, X_c being the central hydrogen content. The results were presented as an average of the three models. The corresponding correction in log k_2 was $-0.87\ \lambda$, larger than that found by Stothers mainly because the three evolutionary phases were taken into account instead of using only homogeneous models. In this paper we try to improve on these results. For this we used the MESA package to generate the standard and rotating models with updated input physics. We computed rotating models for stellar masses from 0.40 $M_\odot$ up to 25.0 $M_\odot$. The corrections by rotation are presented for each mass individually for three evolutionary phases, $X_c = 0.696$, 0.35, and 0.05, which makes the correction process easier and more efficient.

The paper is organized as follows. Section 2 is dedicated to analysing how some physical processes involved in the stellar evolutionary models impact the calculations of log k_2 using homology transformations. Section 3 is devoted to briefly describing the code of stellar evolution as well as the differential equations taking into account the effects of rotation. In Sect. 4 we describe the procedure to integrate the Radau differential equation and analyse the effects of rotation on the stellar structure for all mentioned models. In the same section we also provide a short practical guide on how to correct log k_2 for the effects of rotation. Finally we briefly comment on other physical phenomena that can play a role in the calculations of the theoretical log k_2.

2. A phenomenological approach to the apsidal motion constant using homology transformations

Before going into the matter of how rotation really impacts the degree of mass concentration of stars in this section, we first derive some simple equations, using homology transformations, which are indicators of the behaviour of log k_2. These equations are useful to understand, at least qualitatively, how some physical processes are involved in the calculation of theoretical apsidal motion constants, such as thermonuclear reactions, equations of state, convection.

As is well known, the Radau differential equation is inversely proportional to the mean mass density (see Eq. (13)). Therefore, we used the mass equation for homologous stars:

$$\rho(x) = \rho_o(x)\left(\frac{M}{M_o}\right)\left(\frac{R}{R_o}\right)^{-3}. \tag{1}$$

Here M is the stellar mass, R the stellar radius, ρ the mass density, and the subscript 'o' their homologous counterparts. The centre of the star is also homologous, and therefore we have $\rho_c \propto \rho_m$, where ρ_c is the central mass density and ρ_m is the mean mass density. Thus, we can assume ρ_c as an indicator of the degree of mass concentration. In fact, both variables, ρ_c and ρ_m, can be used as indicators of the behaviour of log k_2.

We adopt the following approximation between the luminosity L and stellar mass M

$$L \propto M^{\chi}, \tag{2}$$

χ ranging from 1.7 for very massive stars up to 3.0 for stars showing masses of the order of 0.5 $M_\odot$. The maximum value of χ is ≈4.6, corresponding to the mass interval 1.0–2.0 $M_\odot$. The average value of χ is ≈3.0. This value also corresponds to homologous stellar models with constant opacity. After some algebra, we have

$$\rho_c \propto M^{\frac{(3\chi-3-2\nu)}{(3+\nu)}}, \tag{3}$$

where ν is the exponent of the thermonuclear energy generation rate, $\epsilon_N \approx \epsilon_o \rho T^\nu$.

The correct values of log k_2 depend on the density distribution according to the Radau equation. However, using the results of homology transformations (Eq. (3)) we can approximately anticipate what the dependence of log k_2 on stellar mass will be. As an example, for a 5.0 $M_\odot$ model we have $\nu \approx 15$ (CNO cycle) and $\chi \approx 3.7$. In this case the corresponding central density ρ_c is proportional to $M^{-1.22}$. For models in the interval 1.0–1.7 $M_\odot$ (pp-chains) $\nu \approx 4$ and $\chi \approx 4.6$ resulting in $\rho_c \propto M^{0.40}$. The difference in these exponents indicates that there is a change in the behaviour of the central mass density and, as a consequence, also in Log k_2 around this mass interval. The dependence on stellar mass is stronger for less massive stars. This feature is confirmed using more realistic models of stellar evolution and the Radau differential equation to compute log k_2. In addition, this mass interval shows interesting features, specifically in the case of the 1.7 $M_\odot$ model. Around this model the mean mass density remains more or less constant. However, for masses lower than ≈1.7 $M_\odot$ the influence of electron degeneracy begins to increase the mean density. Using more elaborate stellar models (see following sections), it can be seen in Fig. 1 that the behaviour of the inverse of the mean density, and therefore of log k_2, is in qualitative accordance with the theoretical predictions coming from the homology transformations since the differential equation by Radau is inversely proportional to the mean mass density (Eq. (13)).

Another way to verify the capability of homology transformations to predict the behaviour of log k_2, at least qualitatively, can be seen in Fig. 2. In this figure the central density (in logarithmic scale) is plotted as a function of mass for zero age mean sequence (ZAMS) non-rotating models computed using

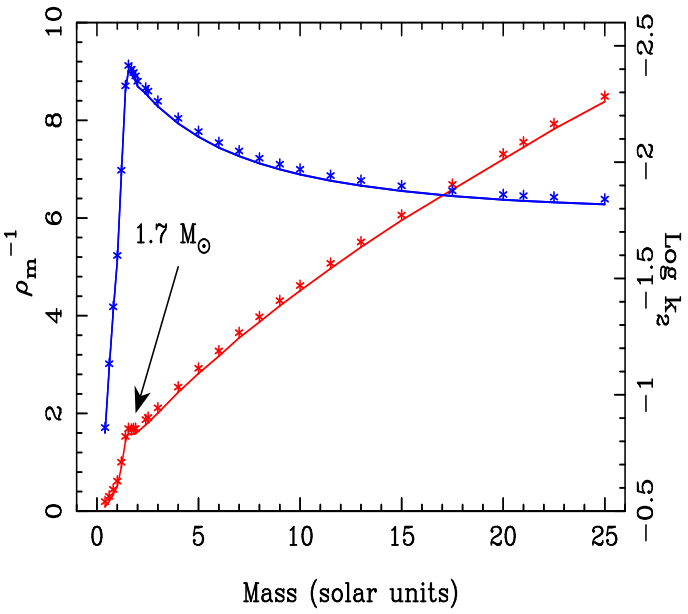

Fig. 1. Apsidal motion constant log k_2 (blue) and the inverse of mean mass density (cm^3 g^{-1}, red) as a function of stellar mass. The models were computed using the MESA package. The corresponding log k_2 values were computed integrating the Radau differential equation using ZAMS (X_c = 0.696) non-rotating models.

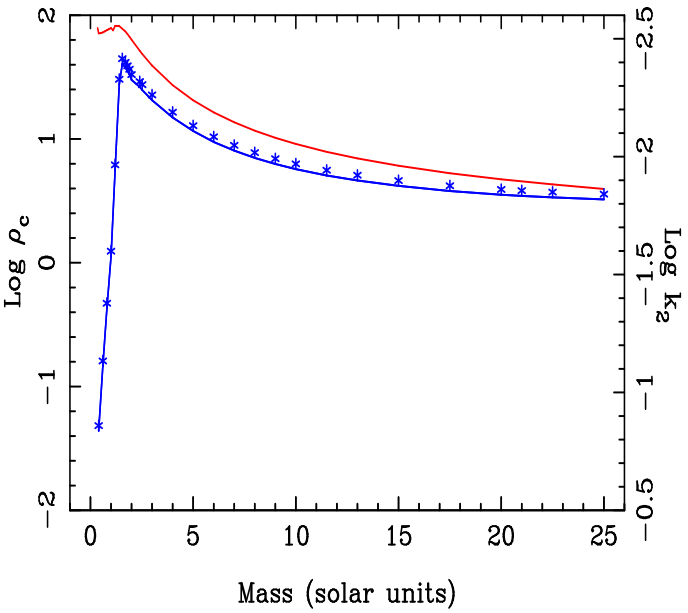

Fig. 2. Apsidal motion constants (blue) and central mass density (red) for the same models as in Fig. 1.

the MESA package. In that figure we have also plotted the apsidal motion constants as a function of mass for comparison. It can be noted that there is a correlation between the central density and log k_2, although not perfect. In the low-mass region a small drop can be seen at around 1.2 $M_\odot$ due to the change in thermonuclear energy processes, that is, CNO to pp-chains. For this range of masses the mass-radius relation also changes due to convection onset at the upper layers. Moreover less massive stars change their behaviour due to the increase in electron degeneracy which plays an important role in the central mass density distribution.

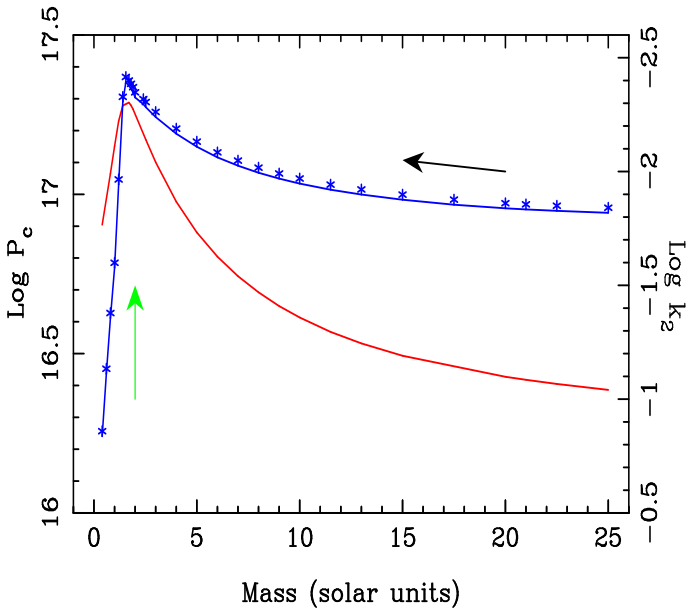

Fig. 3. Apsidal motion constants (blue) and central pressure (red) for the same models as in Fig. 1. The black arrow ($M \gtrapprox 1.7\,M_\odot$) and the green arrow ($M \lessapprox 1.7\,M_\odot$) indicate schematically the effects of rotation on log k_2.

As previously mentioned, the change in the exponent in Eq. (3), and therefore in log k_2, predicted by homology transformations around the interval 1.5–1.7 $M_\odot$ is detected using more elaborate models (Figs. 1 and 2). The morphology of these figures shows another interesting aspect: the input physics are very different for the 10.0 $M_\odot$ and 1.2 $M_\odot$ models (e.g. thermonuclear reactions, equation of state, range of opacities, convection), but both models present the same mass distribution at the ZAMS. This feature extends to other mass pairs.

A uniformly rotating stellar model with mass M presents central properties, for example pressure or density, similar to those of a non-rotating model, but with mass $M - \Delta M$, where $\Delta M > 0$. This characteristic is the mass-lowering effect (see Sackmann 1970; Tassoul 2000). More recently Sirotkin & Woong-Tae (2009) used a self-consistent field method to investigate the effects of rotation and tidal perturbations adopting polytropic models. We anticipate that such effects are not very large, even for fast rotating models. Therefore, we expect the impact on log k_2 to be small, although not negligible. Such an effect can be useful to qualitatively understand how rotation affects the calculations of log k_2. In Fig. 3 we show the central pressure for non-rotating models as a function of stellar mass. The central pressure always increases from 25.0 $M_\odot$ to the 1.5–1.7 $M_\odot$ interval, where a change in the trend appears. A black arrow indicates the direction that stellar models would respond under the effects of rotation, that is, they emulate lower-mass models showing smaller log k_2 (more mass concentrated). This effect, referring to more realistic models depends on the mass, on the evolutionary status, and on the values of initial angular velocities.

On the other hand, non-rotating models with masses lower than 1.5–1.7 $M_\odot$ show central pressures increasing with stellar mass. For this mass interval the corresponding rotating models show central pressures lower than their counterpart non-rotating models. Such an effect occurs mainly due to the cross-over of thermonuclear reactions from the CNO cycle to pp-chains. The green arrow in Fig. 3 indicates the same idea

as the black arrow, but for lower-mass models. Both arrows indicate, schematically, how rotation increases the degree of mass concentration. We confirm this point in the next subsection adopting more realistic stellar evolutionary models. The central temperature decreases for the whole grid of rotating models studied here, and is more pronounced for the 0.40–1.7 $M_\odot$ interval.

3. The evolutionary tracks: rotating models

The stellar evolutionary models were computed using the Modules for Experiments in Stellar Astrophysics package (MESA version r-10398; see Paxton et al. 2019). For the opacities we adopted the element mixture given by Asplund et al. (2009), while for the initial chemical composition we used a generic mixture: $X = 0.700$ and $Z = 0.02$. We adopted for the mixing-length parameter $\alpha_{\rm MLT}$ the value 1.84, the solar calibrated value (option 'Henyey'; see Torres et al. 2015). The present models were followed from the pre-main sequence up to the phase where the central hydrogen content decays to 0.03 or less, covering most of the masses and evolutionary stages of DLEBSs showing apsidal motion (Claret et al. 2021; Table 1).

We do not expect the effects of rotation on the degree of mass concentration to be very large for main-sequence systems, as discussed in Sect. 2. However, considering the current precision with which the absolute dimensions and apsidal motion rates for DLEBSs are measured and the capability of modern stellar evolution codes, we think it is necessary to introduce the corresponding corrections by rotation. We do not consider here the effects of core overshooting and mass loss to highlight only the effects of rotation, given that core overshooting can be considered as a first-order effect concerning $\log k_2$ (for the specific effects of core overshooting and mass loss on $\log k_2$, see e.g. Claret & Giménez 1991; Claret & Torres 2019).

The most representative characteristic of a stellar model under the effects of rotation is the loss of symmetry, resulting in an oblate configuration. In a rotating model the centrifugal forces increase the equatorial radius, while the polar radius is reduced, but on a smaller scale. As a consequence, the mean radius of the configuration is larger than that of a non-rotating model with the same mass. On the other hand, in a rotating model the average and central mass density and pressure must change to compensate the centrifugal and pressure gradients. This has direct consequences on the behaviour of $\log k_2$, the rotating models being more mass concentrated than their corresponding standards, as we discuss in the next paragraphs.

For a star rotating rigidly in hydrostatic equilibrium, the Roche potential can be written as

$$\Psi(r,\theta) = \Phi(r,\theta) - \frac{1}{2}\Omega^2 r^2 \sin^2\theta. \tag{4}$$

In this equation $\Phi(r,\theta)$ is the Newtonian potential, Ω is the angular velocity, and θ is the colatitude. Under such conditions the isobars coincide with equipotential surfaces. The differential equations of stellar structure are changed by rotation as follows:

$$\frac{\partial r_\psi}{\partial M_\psi} = \frac{1}{4\pi\rho r_\psi^2}, \tag{5}$$

$$\frac{\partial P_\psi}{\partial M_\psi} = -\frac{GM_\psi}{4\pi r_\psi^4} f_P - \frac{1}{4\pi\rho r_\psi^2}\left(\frac{\partial^2 r_\psi}{\partial t^2}\right), \tag{6}$$

$$\frac{\partial L_\psi}{\partial M_\psi} = \epsilon_N - \epsilon_\nu + \epsilon_{\rm gravi}, \tag{7}$$

$$\frac{\partial \ln T_\psi}{\partial \ln P_\psi} = \frac{3\kappa L_\psi P_\psi}{16\pi acGM_\psi T_\psi^4}\frac{f_T}{f_P}\left[1 + \frac{r_\psi^2}{GM_\psi f_p}\frac{\partial^2 r_\psi}{\partial t^2}\right]^{-1}. \tag{8}$$

The factors f_P and f_T are calculated according to the following equations:

$$f_P = 4\pi r_\psi^4 \frac{1}{GM_\psi S_\psi \overline{g^{-1}}}, \tag{9}$$

and

$$f_T = \left(\frac{4\pi r_\psi^2}{S_\psi}\right)^2 \frac{1}{\overline{g}\,\overline{g^{-1}}}, \tag{10}$$

where r_ψ is the equivalent radius of an isobar; M_ψ is the mass inside such an isobar; S_ψ is its surface area; M_ψ and L_ψ are the mass and luminosity enclosed by an equipotential; ϵ_N, $\epsilon_{\rm gravi}$, and ϵ_ν are respectively the nuclear nuclear energy generation rate per unit mass, gravitational heating rate, and neutrino loss rate; κ is the opacity; T_ψ and P_ψ are the temperature and pressure; ρ is the density, a is the radiation pressure constant; and c is the velocity of light in a vacuum. The overlined quantities indicate that the mean values of local gravity and its inverse are taken over equipotentials. For non-rotating models, f_T and $f_P = 1.0$, as expected. It is interesting to note that we can write the equation for r as

$$r = a\,(1 - f_2 P_2(\cos\theta))\,, \tag{11}$$

where a (not to be confused with a, the radiation pressure constant) is the radius of the level surface and $P_2(\mathrm{Cos}\theta)$ is the second Legendre polynomial and

$$f_2 = \frac{5\Omega^2 a^3}{3GM_\psi(2+\eta_2)}, \tag{12}$$

where η_2 is directly connected with Radau equation. We note that k_j depends on $\eta(R)$ (see Eq. (18)). More technical details on f_P and f_T calculations can be found in Kippenhahn & Thomas (1970) and Endal & Sofia (1976).

Here we adopt for our rotating models the solid body rotation approach (i.e. the angular velocity is the same throughout the model). We computed grids of rotating and standard models for the interval 0.40 $M_\odot$–25.0 $M_\odot$ in order to cover the range where apsidal motion has been detected and measured with sufficient accuracy in DLEBSs. To evaluate the effects of stellar rotation on the internal structure and in particular on $\log k_2$, firstly a non-rotating model is computed for each mass to be taken as a reference. In the next step, models with variable rotation rates are computed, provided that such rotational velocities are not close to the break-up values. The differences between the respective $\log k_2$, e.g. $[\log k_{2\ \rm rotating} - \log k_{2\ \rm standard}]$, are calculated for three phases of stellar evolution: $X_{\rm c} = 0.696$ (ZAMS), 0.35, and 0.05 covering the mass range and evolutionary stages of DLEBSs showing apsidal motion (see Table 1 in Claret et al. 2021).

4. The computation of k_2, k_3, and k_4

The theoretical apsidal motion constants k_2, k_3, and k_4 were computed simultaneously by integrating numerically the Radau equation for all models, instead of using the original Clairaut

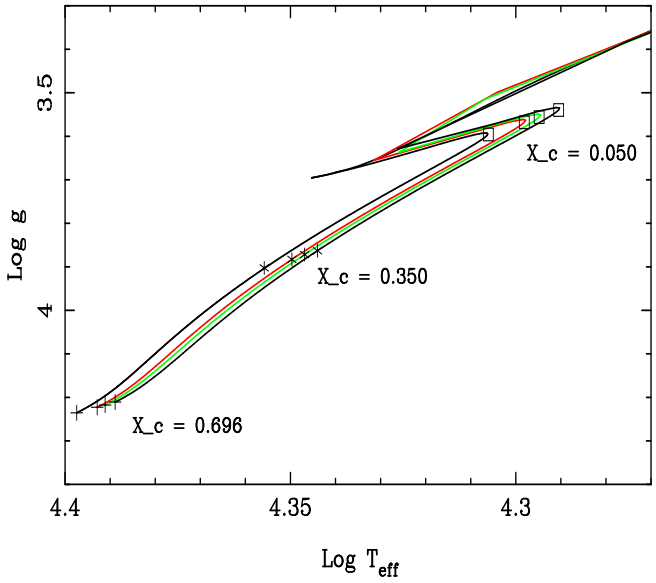

Fig. 4. Standard model and some rotating models for 10.0 $M_{\odot}$. The black line indicates non-rotating models. The red line represents models with $\omega_{\rm initial}$ at the ZAMS = 6.0×10^{-5} s^{-1}, the green line represents the models with $\omega_{\rm initial}$ = 7.0×10^{-5} s^{-1}, while the blue line indicates the model with $\omega_{\rm initial}$ = 8.0×10^{-5} s^{-1}. The plus signs (+), asterisks (∗), and squares (□) represent the evolutionary phases $X_{\rm c}$ = 0.696, 0.35, and 0.05, respectively. For the sake of clarity only three rotating models are shown.

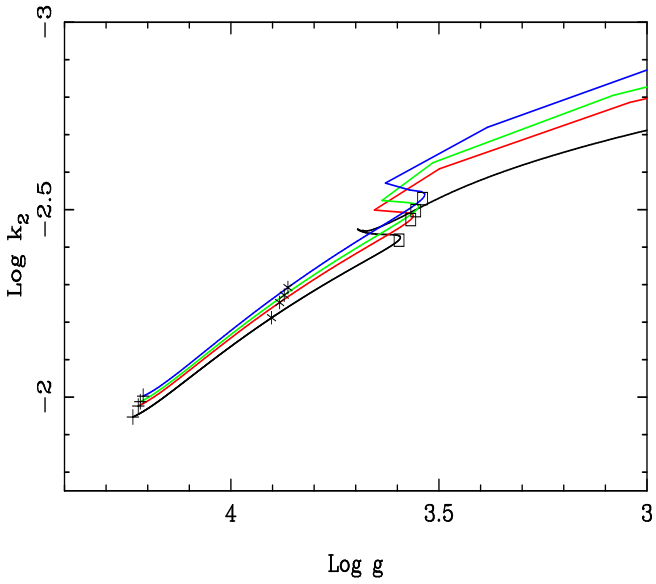

Fig. 5. Effects of rotation on log k_2 as a function of log g for the same models and symbols shown in Fig. 4.

equation. We adopted a fifth-order Runge-Kutta method and a tolerance level of 10^{-7}. The Radau differential equation is given by the following expression (Kopal 1959):

$$\frac{a{\rm d}\eta_j}{{\rm d}a} + \frac{6\rho(a)}{\overline{\rho}(a)}(\eta_j+1) + \eta_j(\eta_j-1) = j(j+1), \quad j = 2,3,4. \quad (13)$$

The auxiliary parameter η_j is given by

$$\eta_j \equiv \frac{a}{\epsilon_j}\frac{{\rm d}\epsilon_j}{{\rm d}a}. \quad (14)$$

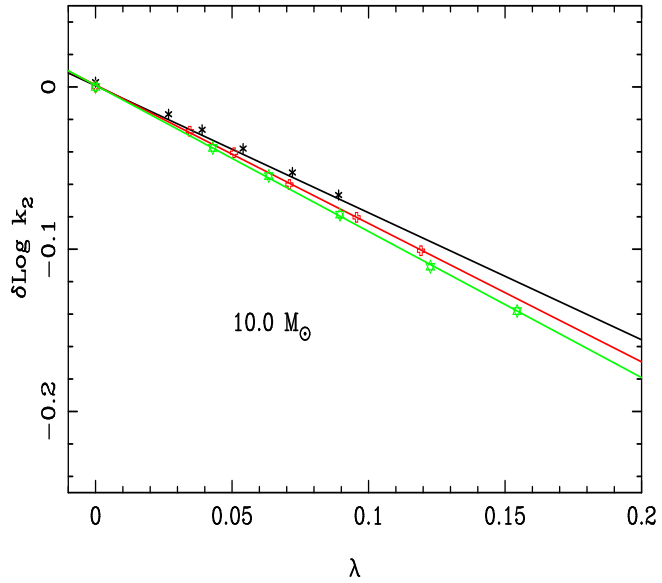

Fig. 6. Effects of rotation on the apsidal motion constant log k_2 as a function of λ. The black asterisks symbolize the evolutionary phase $X_{\rm c}$ = 0.696, red crosses $X_{\rm c}$ = 0.35, and green stars $X_{\rm c}$ = 0.05. The calculations are for the 10.0 $M_{\odot}$ models.

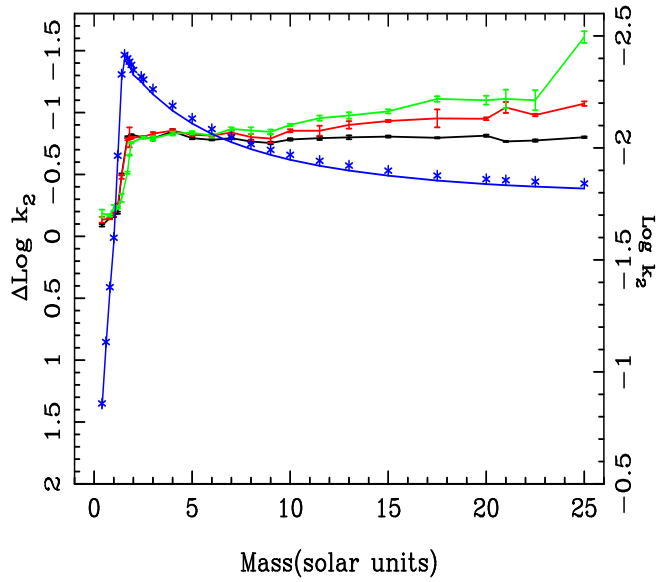

Fig. 7. Effects of rotation on the apsidal motion constant log k_2 as a function of model mass. The black line symbolizes the evolutionary phase $X_{\rm c}$ = 0.696, the red line $X_{\rm c}$ = 0.35, and the green line $X_{\rm c}$ = 0.05. The slopes for each mass here come from the analysis of the effects of rotation on log k_2, as shown in Fig. 6; see also Table 1. As a reference, the apsidal motion constants for the ZAMS (non-rotating models) is represented by a blue line. For the sake of clarity only three rotating models are shown.

In the above equations a denotes the mean radius of the stellar configuration, ϵ_j is a measure of the deviation from sphericity, $\rho(a)$ is the mass density at the distance a from the centre of the configuration, and $\overline{\rho}(a)$ is the mean mass density within a sphere of radius a. The boundary conditions for this differential equation are, following Poincaré (1902),

$$\left(\frac{{\rm d}\eta}{{\rm d}a}\right)_{\eta=0} = -\frac{3(j-1)}{j+1}\frac{{\rm d}D}{{\rm d}a}, \quad (15)$$

Table 1. Slopes for Eq. (19).

Mass ($M_\odot$)	log g	Δlog k_2 (M, X_c = 0.696)	log g	Δlog k_2 (M, X_c = 0.35)	log g	Δlog k_2 (M, X_c = 0.05)
0.4	4.913	−0.093 ± 1.41e−2	4.849	−0.137 ± 3.20e−2	4.688	−0.192 ± 4.14e−2
0.8	4.620	−0.146 ± 2.73e−3	4.547	−0.145 ± 6.93e−3	4.413	−0.170 ± 1.00e−2
1.0	4.535	−0.170 ± 1.38e−2	4.437	−0.179 ± 1.86e−2	4.329	−0.231 ± 2.31e−2
1.2	4.397	−0.191 ± 8.70e−3	4.283	−0.252 ± 1.31e−2	4.166	−0.234 ± 1.14e−2
1.4	4.285	−0.501 ± 7.45e−3	4.129	−0.480 ± 1.51e−2	4.009	−0.311 ± 3.27e−2
1.7	4.285	−0.802 ± 6.75e−3	4.045	−0.785 ± 8.00e−3	3.824	−0.514 ± 9.36e−3
1.8	4.291	−0.793 ± 6.38e−3	4.037	−0.800 ± 8.02e−2	3.786	−0.656 ± 4.30e−3
1.9	4.298	−0.821 ± 3.27e−3	4.028	−0.797 ± 8.44e−3	3.763	−0.758 ± 5.97e−3
2.52	4.300	−0.799 ± 7.57e−3	3.991	−0.804 ± 7.46e−3	3.703	−0.799 ± 7.22e−3
3.0	4.296	−0.792 ± 1.68e−2	3.971	−0.829 ± 1.25e−2	3.677	−0.792 ± 1.50e−2
4.0	4.282	−0.847 ± 1.86e−2	3.953	−0.854 ± 1.10e−2	3.659	−0.830 ± 1.42e−2
5.0	4.272	−0.793 ± 8.10e−3	3.944	−0.820 ± 8.87e−3	3.656	−0.837 ± 1.30e−2
6.0	4.263	−0.780 ± 4.65e−3	3.934	−0.814 ± 7.80e−3	3.643	−0.814 ± 1.56e−2
7.0	4.254	−0.793 ± 8.11e−3	3.925	−0.839 ± 1.51e−2	3.636	−0.868 ± 1.27e−2
8.0	4.248	−0.766 ± 1.49e−2	3.916	−0.802 ± 2.41e−2	3.624	−0.855 ± 2.60e−2
9.0	4.241	−0.754 ± 1.03e−2	3.911	−0.790 ± 3.46e−2	3.609	−0.844 ± 1.89e−2
10.0	4.236	−0.783 ± 9.02e−3	3.902	−0.853 ± 1.21e−2	3.596	−0.900 ± 9.14e−3
11.5	4.228	−0.793 ± 1.40e−2	3.888	−0.853 ± 4.06e−2	3.571	−0.955 ± 2.10e−2
13.0	4.221	−0.800 ± 1.54e−2	3.880	−0.900 ± 3.00e−2	3.543	−0.976 ± 2.63e−2
15.0	4.214	−0.806 ± 7.86e−3	3.867	−0.932 ± 8.68e−3	3.507	−1.010 ± 1.66e−2
20.0	4.200	−0.813 ± 8.56e−3	3.834	−0.950 ± 1.10e−2	3.418	−1.100 ± 3.58e−2
21.0	4.198	−0.767 ± 4.56e−3	3.829	−1.041 ± 4.43e−2	3.397	−1.110 ± 7.50e−2
22.5	4.194	−0.774 ± 9.13e−3	3.817	−0.980 ± 1.00e−2	3.352	−1.100 ± 8.04e−2
25.0	4.188	−0.801 ± 6.39e−3	3.808	−1.072 ± 1.78e−2	3.336	−1.612 ± 4.76e−2

Notes. The content of this table is as follows: Col. 1 indicates the mass of the model in solar units; Col. 2 the log g corresponding to X_c = 0.696; Col. 3 the slope for this evolutionary phase; Cols. 4, 5 and 6, 7 indicate the same, but for the evolutionary phases X_c = 0.35 and 0.05, respectively.

where

$$D = \frac{\rho(a)}{\overline{\rho}(a)} \tag{16}$$

and

$$\eta_j(0) = j - 2. \tag{17}$$

Finally, the apsidal motion constant of order j is given by

$$k_j = \frac{j + 1 - \eta_j(R)}{2\left(j + \eta_j(R)\right)}, \tag{18}$$

where $\eta_j(R)$ indicates the values of η_j at the surface of the star.

In Fig. 4 we can see the effects of rotation on the Hertzsprung–Russell (HR) diagram for 10.0 $M_\odot$ models. Rotating models present lower effective temperatures as well as larger equivalent radii (see e.g. Sect. 2). The net effect of rotation is a broader and longer main-sequence lifetime. Concerning log k_2, Fig. 5 illustrates for the same models, the differences between non-rotating and rotating models. Such differences increase with evolutionary stage and with the values of $\omega_{\rm initial}$. The influence of rotation on k_2 can mainly be noted for X_c = 0.05.

Figure 6 shows an example of the procedure to relate the rotating and the standard models in the case of the 10.0 $M_\odot$ models. The quantities δLog k_2 = [Log $k_{2\ \rm rotating}$ − Log $k_{2\ \rm standard}$] are plotted as a function of λ. We note that λ can also be written as $\lambda = \Omega^2/(2\pi G\rho_{\rm m})$; see previous discussion on the role of $\rho_{\rm m}$ in the degree of stellar mass concentration in Sect. 1. The behaviour of δLog k_2 is linear for the adopted angular velocities. All models of the present grid show a similar behaviour and provide a similar quality of fits. The impact on the models distorted by rotation can be seen in Fig. 6: the larger the initial rate of rotation, the larger the difference between the standard model and its rotating counterparts concerning log k_2, the corresponding rotating models being more mass concentrated than the non-rotating ones.

Figure 7 shows the resulting slopes, ΔLog k_2, for three evolutionary phases, X_c = 0.696 (black line), X_c = 0.35 (red line), and X_c = 0.05 (green line) as a function of stellar mass. The values of log k_2 are shown for reference (ZAMS, non-rotating models). Figure 7 shows some interesting features. For low-mass stellar models the slope increase with mass up to the 1.7–1.8 $M_\odot$ interval, qualitatively in agreement with that predicted by Eq. (3). For more massive stars, the behaviour of the slopes is smoother, also consistent with Eq. (3). In general the slopes for more evolved phases are larger than for models located in the ZAMS phase. There are some exceptions around 1.7 $M_\odot$. For this model and the 1.8 $M_\odot$ model the slope for X_c = 0.05 is smaller than that for X_c = 0.35, whereas for the 1.9 $M_\odot$ model such differences decrease. For a 2.52 $M_\odot$ model the three slopes are practically the same (see previous discussion on this mass interval in Sect. 2).

5. A short guide to correct the theoretical log k_2 by the effects of rotation

Before applying the corrections due to rotation presented here, it is necessary to use the standard stellar models (i.e. non-rotating models that include the effects of core overshooting and mass loss). To obtain the non-rotating values of log k_2 as a function of mass, evolutionary stage, and chemical composition see Claret (2019, 2023) and Claret & Torres (2019), for example.

The rotating models by Claret (1999) considered only three models: 2.0, 7.0, and 15.0 $M_\odot$ and the corrections for these three models were considered together and not individually as in this paper. The calculations presented here are more efficient and realistic for correcting the theoretical apsidal motion by the effects of rotation for both stars of a given DLEBS as a function of their masses and their evolutionary status (X_c or log g). The slopes for these fittings [$\Delta \mathrm{Log}\, k_2\, (M, \log g, X_c)$] and their respective error bars are displayed in Table 1. To obtain the values of the slopes for the vast majority of DLEBSs it will be necessary to interpolate in Table 1 using the stellar mass and log g (or X_c) as independent variables. For practical purposes the effects of rotation can be incorporated directly into the theoretical analysis of apsidal motion for both components of a given DLEBS using Eq. (19) and the data shown in Table 1. This equation is defined by

$$\log\ k_{2\ \mathrm{rotating}} = \log\ k_{2\ \mathrm{standard}} + \Delta \log\ k_2(M, \log g)\ \lambda. \tag{19}$$

Specific calculations for a given DLEBS can be also carried out on request.

Finally, some remarks on other effects of second-order on log k_2. The present calculations were carried out in the framework of static tides. However, if the orbital period is smaller than the periods of free oscillation modes, another formalism is necessary: the dynamic tides. This is due to the effects of the compressibility of the stellar fluid and is particularly important if the components of a DLEBS are nearly synchronized. Furthermore, in the case of higher rotational angular velocities, additional deviations due to resonances appear if the forcing frequencies of the dynamic tides are in the range of the free oscillation modes of both stars. Such mechanisms were studied by Claret & Willems (2002), Willems & Claret (2003), and Claret et al. (2021), and the references given in these papers. The correction due to the effects of dynamical tides is given by the following equation:

$$\Delta_{\mathrm{dyn}} = \left[k_{2\,\mathrm{standard}} - k_{2\,\mathrm{dyn}}\right] / k_{2\,\mathrm{dyn}}. \tag{20}$$

For example, the correction for the case of EM Car is ≈3% of the total k_2.

Acknowledgements. This paper is dedicated to the memory of R. D. Tarsia, teacher and friend. I thank an anonymous referee for his/her pertinent comments and suggestions that have improved this paper. The Spanish MINC/AEI (PID2022-137241NB-C43 and PID2019-107061GB-C64) are gratefully acknowledged for their support during the development of this work. AC also acknowledges financial support from the grant CEX2021-001131-S funded by MCIN/AEI/10.13039/501100011033. This research has made use of the SIMBAD database, operated at the CDS, Strasbourg, France, and of NASA's Astrophysics Data System Abstract Service.

References

Asplund, M., Grevesse, N., Sauval, A. J., & Scott, P. 2009, ARA&A, 47, 481
Claret, A. 1999, A&A, 350, 56
Claret, A. 2019, A&A, 628, A29
Claret, A. 2023, A&A, 674, A67
Claret, A., & Giménez, A. 1991, A&A, 244, 319
Claret, A., & Giménez, A. 1993, A&A, 277, 487
Claret, A., & Torres, G. 2019, ApJ, 876, 134
Claret, A., & Willems, B. 2002, A&A, 388, 518
Claret, A., Giménez, A., Baroch, D., et al. 2021, A&A, 654, A17
Endal, A. S., & Sofia, S. 1976, ApJ, 210, 184
Kippenhahn, R., & Thomas, H. C. 1970, in Proc. IAU Coll. 4, Stellar Rotation, ed. A. Slettebak (Philadelphia, PA: Gordon & Breach), 20
Kopal, Z. 1959, Close Binary Systems (London: Chapman and Hall), 29
Paxton, B., Smolec, R., Schwab, J., et al. 2019, ApJS, 243, 10
Poincaré, H. 1902, in Leçons sur les Figures d'Equilibre d'une masse fluide (lectures at the Sorbonne), ed. L. Dreyfus (Carré et Naud, Paris), 9
Sackmann, I. J. 1970, A&A, 8, 76
Sirotkin, F. V., & Woong-Tae, K. 2009, ApJ, 698, 715
Stothers, R. 1974, ApJ, 194, 651
Tassoul, J. L. 2000, in Stellar Rotation, (New York: Cambridge University Press), Cambridge Astrophys. Ser., 36
Torres, G., Claret, A., Pavlovski, K., & Dotter, A. 2015, ApJ, 807, 26
Willems, B., & Claret, A. 2003, A&A, 410, 289